(2)

FINAL REPORT

ON

Basic Studies in Turbulent Shear Flows

Sponsored by

Office of Naval Research

Contract Number N00014-89-J-1361

Scientific Officer: Dr. L. Patrick Purtell
Fluid Dynamics Program (1132F)
800 N. Quincy Street
Arlington, VA 22217-5000

Principal Investigator

Fazle Hussain
Cullen Distinguished professor
Mechanical Engineering Department
University of Houston, Houston, TX 77204-4792

March 2, 1992

Final Report
on
Basic Studies in Turbulent Shear Flows

The primary goal of this research was to provide improved understanding of basic physical phenomena in fluid mechanics, particularly in transitional and turbulent flows. Key to this understanding, we believe, is the concept of *coherent structures*. If we understand the dynamics of coherent structures, then we may predict and possibly affect flow dynamics in technologically useful ways. Therefore, our research is focused on the measurement, understanding, modeling, prediction, and finally manipulation of coherent structures in transitional and turbulent shear flows. Significant results we have achieved are discussed in the following.

1. Subharmonic Resonance in Free Shear Layers

Our study of subharmonic resonance phenomenon in free shear layers and jets has given us a better understanding of the fundamentals of the nonlinear phenomenon and control of turbulence in jets and shear layers using excitation. Experiments were performed in a carefully documented and controlled initially laminar, single-stream shear layer using phase-locked, two-frequency excitation applied at the origin of the shear layer. The excitation signal consisted of a fundamental frequency f and its subharmonic f/2, with a controllable initial phase angle ϕ_{in} between the two. Effects of $St_{\theta e}$ ($\equiv f\theta_e / U_c$), phase angle ϕ_{in}, amplitudes of excitation, and detuning on the evolution of the subharmonic were studied. The evolution of the subharmonic shows strong dependence on ϕ_{in}. However, at the location of saturation of the fundamental, the phase angle ϕ between the fundamental and the subharmonic is zero for maximum attenuation and $\pi/2$ for maximum enhancement of the subharmonic, irrespective of the $St_{\theta e}$ value. We denote the phase angles which result in maximum attenuation and enhancement of the subharmonic as ϕ_{at} and ϕ_{en} respectively. The present study has allowed us to confirm quantitatively why a natural shear layer rolls up at $St_{\theta e} \approx 0.012$ (Zaman & Hussain 1980) instead of the theoretical value of the most unstable Strouhal number of $St_{\theta e} \approx 0.017$. This apparent contradiction is believed to be a consequence of the feedback caused by the induced velocity of rolled-up vortices being strongest at $St_{\theta e} \approx 0.012$ (Hussain 1986).

Instead of explaining hot-wire data, here we show flow visualization pictures which reveal clearly the mode of interaction. Figure 1.1(a,b) shows the sequence of interactions for ϕ_{en} and ϕ_{at}, where ϕ_{en} and ϕ_{at} denote the phases which produce maximum enhancement and attenuation respectively of the subharmonic. In these two cases, subharmonic excitation was maintained at a lower level than the fundamental. At ϕ_{en}, two vortices roll up close to each other, and subsequently pair (figure 1.1a). On the other hand, at ϕ_{at}, equally spaced vortices form and advect downstream almost in a straight line (figure 1.1b). However, the imposed initial excitation condition is incapable of maintaining the unstable straight-line configuration of vortices farther downstream. Ambient disturbances presumably are sufficient to destroy this configuration, and the vortices either break down or undergo pairing randomly in space and time.

We found that shredding occurs in the case of strong subharmonic excitation at ϕ_{at}. Shredding refers to the situation when a weak vortex falls between two equally spaced, stronger vortices; the latter two shear the former into a sheet and pull it apart. Because of the straining action of the two neighboring stronger vortices, vorticity from the weaker middle vortex is transported to the neighboring upstream and downstream vortices. A sequence of flow visualization pictures of the shredding interaction is shown in figure 1.2(b). Small deviations from the phase difference ϕ_{at} inhibit shredding and initiate pairing (figure 1.2a).

2. Spatiotemporal Dynamics of Free Shear Flows

We have continued our investigations of driven free shear flows as dynamical systems. We have come to understand that the key issue is sensitivity of the fluid dynamical system to external noise (dynamically open) rather than mass flux through the system (physically open). Since many free shear flows are convectively unstable, they are dynamically open. However, closure is achieved by feedback from significant downstream events such as coherent structure formation or interaction (*e.g.*, vortex pairing). Without this dynamical closure, these systems should not be expected to behave as temporal dynamical systems. With it, however, standard techniques for analysis are applicable. We have explored periodically forced transitional jets. Our investigations of the 2-D parameter space ($a_f = u'_f/U_e$, $St_D = fD/U_e$) has revealed 2 periodic attractors (stable vortex pairing, SP and stable double pairing, SDP) and two other interesting attractors: a chaotic attractor (CA) in the region $1.1 \leq St_D \leq 1.3$ and a nearly periodically modulated attractor (NPM) in the region $0.6 \leq St_D \leq 0.75$. In all cases reported here, the fundamental frequency f = 264

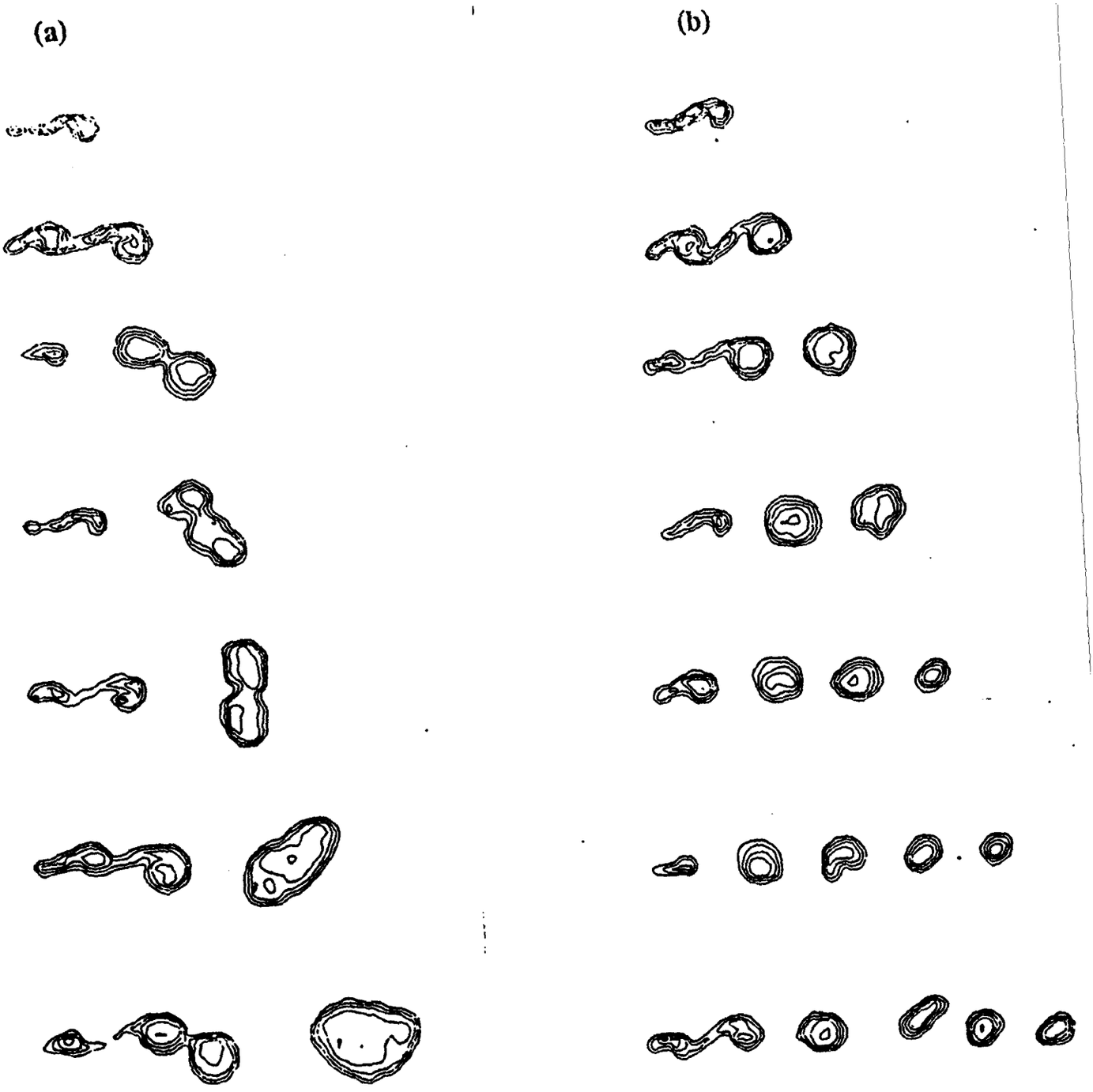

Figure 1.1 Digitally processed flow visualization data (iso-intensity contours) showing sequence of coherent structure interactions. (a) Enhancement of pairing; (b) suppression of pairing.

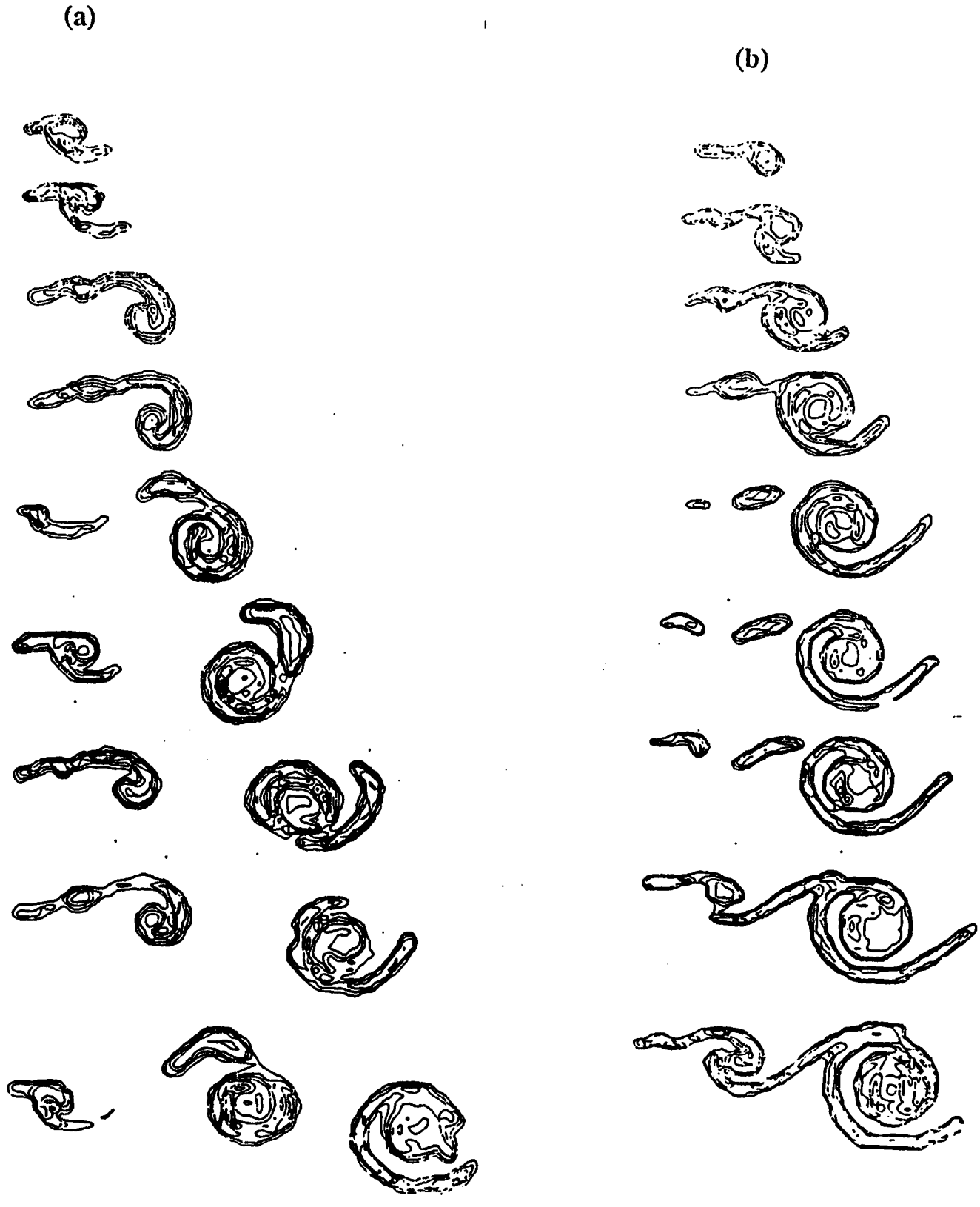

Figure 1.2 Digitally processed flow visualization data (iso-intensity contours) showing sequence of coherent structure interactions. (a) Enhancement of pairing; (b) shredding interaction.

Hz; bands at f/2 and f/4 are due to pairing and double pairing respectively. These attractors are discussed below.

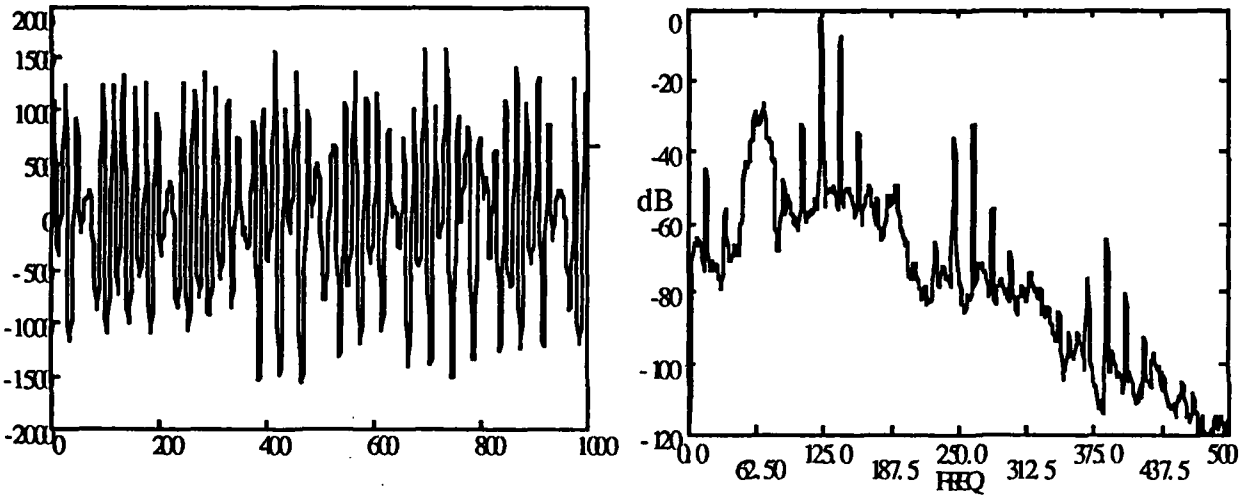

Figure 2.1: Signal and Spectrum of Chaotic Attractor

Figure 2.1 shows two characteristic signatures of the chaotic attractor: (i) the signal is very strongly, but chaotically modulated, and (ii) the spectrum has sharp modulation sidebands around f/2, a broader band around f/4 due to chaotic modulation, and a well-filled background spectrum falling off at higher frequencies. Estimates of dimension ($\nu \cong 3$), largest Lyapunov exponent ($0.2 \leq \lambda_1 \leq 0.5$) and Kolmogorov entropy ($0.3 \leq KE \leq 0.6$) indicate that this attractor is chaotic. Transitions can be hysteretic; jumps occur to and from CA and another less distinctive modulated state at different values of a_f, depending on whether a_f is being increased or decreased. Transitions from CA to SDP are intermittent, alternating between states.
The characteristic trace and spectrum of NPM are shown in figure 2.2. The self-modulations of vortex pairing occur almost periodically. The spectrum, therefore, shows sharp sidebands at $f/2 \pm \Delta f$, $\Delta f \cong 3.5$ Hz. However, there is some broadening of the spectral peaks and some filling of the background. The characterization of the attractor is not so distinct: (i) the dimension $\nu > 2$, actually having two scaling regions develop in the correlation dimension calculation, and (ii) λ_1 and KE values depend upon which scaling region is chosen for analysis, being positive for smaller scales and approximately zero for larger scales. It appears that this attractor is found very near the boundary of a quasiperiodic-chaotic transition, but it is found in only a very narrow band in parameter space, making further investigation more difficult. The transition to this state from SP appears to be due to a tangent bifurcation, based on phase-angle return maps of SP and NPM.

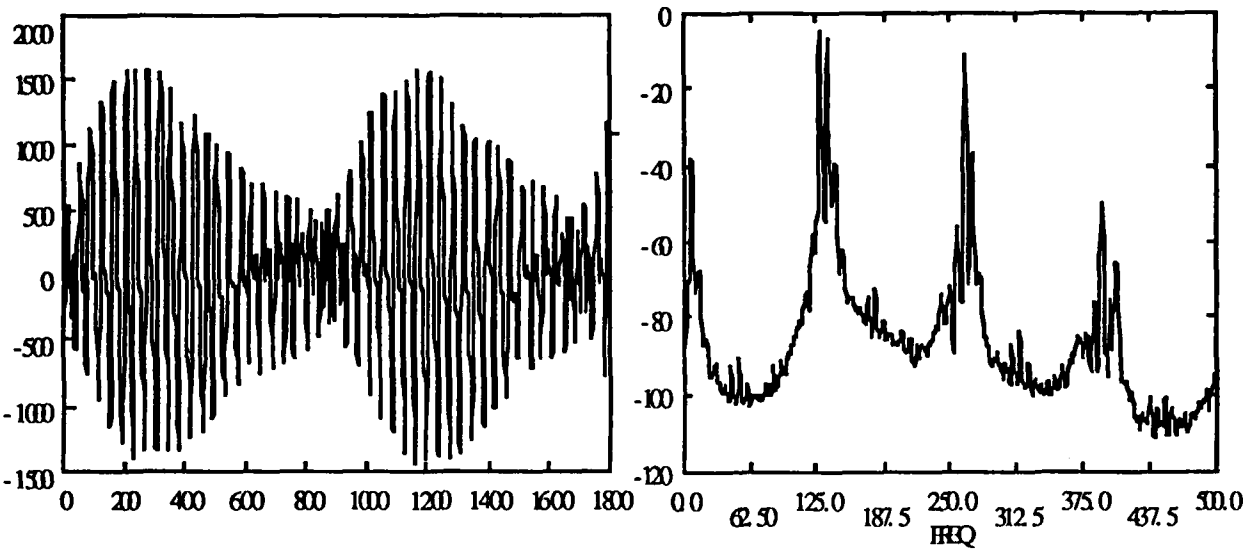

Figure 2.2: Signal and Spectrum of Modulated Attractor

The documentation of these attractors is important because it clearly demonstrates the degree to which the jet transition region behaves as a low-dimensional, deterministic dynamical system with periodic and chaotic attractors and known transitions from one state to another. Additional work is necessary to increase the degrees of freedom in these systems to see how far dynamical closure and low-dimensional temporal behavior can be extended. This will be continued in the upcoming year.

3. Dynamical Systems Tools for Multiple Data Streams

We have extended the embedding techniques used to compute mutual information, correlation dimension, largest Lyapunov exponent and Kolmogorov entropy to incorporate multiple streams of input data. In this way, we can use several variables measured at a single point or variables measured at a number of points in the flow in order to characterize attractors. This will allow us to include some spatial dependence and open a path to investigate spatially developing flows where dynamical closure is weak.

4. Dynamics of Transitional Pipe Flow

Slug flow in a pipe having a smooth, relatively undisturbed entry flow is another example of a flow system which is "open" in the sense that mass crosses the system boundaries (*i.e.*, fluid enters and exits the pipe continuously) yet can be

"closed" in the dynamical sense (as above). This closing of the flow system is achieved by constraining the pressure difference between the pipe inlet and exit to be constant (or at least very nearly so). This results in a strong feedback mechanism wherein the formation and subsequent growth of a turbulent slug causes a reduction in the mass flow rate, which in turn causes the entering fluid to remain laminar until the slug exits the pipe, accelerating the flow and triggering the formation of a new slug. The flow itself is convectively unstable — slugs propagate down the pipe and eventually wash out — but the feedback due to the constraint of the constant pressure difference closes the flow in the dynamical sense.

We have also determined that nonperiodic slugging results when the pressure difference between the pipe inlet and exit is either poorly controlled or not controlled at all. In such a case, the feedback mechanism which would cause periodic slugging is ineffective, and the flow is essentially noise-driven.

We noted that the dimensionless slugging frequency $F^* \equiv f\,L/U$ should properly be used in place of the more commonly used $f\,D/U$. We further observed that the Stokes number $S^* \equiv (D/2)\sqrt{(2\pi f/\nu)}$ for naturally-occurring periodic slug flow usually coincided with the Stokes number range for which Stettler & Hussain (1986) found flow stabilization (*i.e.*, delayed transition) in periodically forced (pulsatile) pipe flow. We have subsequently determined that, although this situation is quite likely to occur, it is in fact coincidental: the possible stabilization/destabilization due to Stokes number effects is largely independent of the natural slugging frequency $F^* \equiv f\,L/U$. Depending on the configuration of the pipe facility, practically any desired value of the Stokes number should be attainable.

A more recent, and possibly far more interesting, observation is that the leading and trailing ends of the slug propagate downstream at velocities which are substantially different from those reported in the literature. More particularly, the velocity of the slug leading end ($U_{LE}/\bar{U}$) is perhaps as much as 60% (or more) greater in our experiments than has been reported elsewhere. Lindgren (1957), Sarpkaya (1966), and Wygnanski & Champagne (1973) all report slug leading (and trailing) end velocities, and are in agreement on a high value of about 1.6 times the bulk velocity. However, a very conservative interpretation of our data gives a result of 2.5, and less-conservative interpretation gives even higher values. One possible explanation is readily apparent: our experiments differed in that they produced periodic slugging, which is associated with fairly high-amplitude mass flow rate oscillations, rather than nonperiodic slugging (which typically occurs when Re is fixed) such as

was observed by the cited researchers. Between the time at which a new slug is generated and the leading interface exits the pipe, the flow is decelerating; we suspect that this deceleration is responsible for the higher slug leading end velocity. We are currently constructing a new facility in which we plan to confirm our measurements and determine the precise mechanism causing this remarkable effect.

5. Eduction of Coherent Structures in the Plane Jet Far Field

Previous work in this field has not yielded a satisfactory account of the coherent structures (if such exist) in the far field of a plane jet. In our lab, a flow visualization study (Schlien & Hussain 1983) and some measurements with a rake of 8 X-wire probes (Jenkinson, Husain, & Hussain 1984) gave some indications of structure, but no adequate detail. Others, such as Mumford (1982), proposed a double-roller structure model from two-point correlation measurements, and Antonia et al (1986) used a rake of X-wires to educe structures in a plane. Based on our own results, we believe that the far-field structures are far more complex (strongly three-dimensional) than proposed by others. In the current work, we are using up to 32 X-wire probes in various configurations to detect and analyze the three-dimensional structures, as noted in the following discussion.

The project consists of three major parts: (a) construction of hardware needed for the measurements; (b) making the measurements and developing the software to process the data; and (c) interpreting the results. Up to this point, we have completed the first task of building three parallel arrays on which the hot-wire stems are mounted. The spacing of the arrays can be adjusted, which enables us to measure two components of the instantaneous velocity in any three planes. Also, our 32 probe stems were constructed in-house; using these in conjunction with our 70 anemometers and 64-channel A/D converter, we are now able to cover a spatial extent large enough to capture the large–scale structures, yet still retain adequate spatial resolution.

Furthermore, the software for data processing is based on the following overview of our philosophy to educe CS. (1) Following our definition of coherent structures as phase-correlated vorticity fields, we use spatial distributions of the instantaneous vorticity field in order to detect the passage of a structure. (2) We then select certain features such as shape, size and strength, and a feature parameter range (*i.e.*, threshold) based on multi-dimensional pdf's that dictate the statistical and dynamical importance of the structure. (3) We finally perform an ensemble

average on the realizations that are accepted after our criteria has been imposed (conditional averaging). Furthermore, cross correlating 2D cuts of the structure (obtained simultaneously from different arrays of X-wires) in the spanwise and transverse directions will enable us to educe the 3D details of the structure.

Some preliminary measurements using two single wires have been made in order to study the characteristics of the initial development of the structures. These consisted of two-point correlation measurements in the jet spanwise direction. We observed that the structure is initially homogeneous in this direction after which it becomes increasingly distorted with downstream distance. The wavelength of this distortion will be used to determine the array spacing for subsequent experiments.

Our next step is to make the final measurements, as follows: (1) Transverse vorticity $\omega_y(z,t)$ distributions along a line in the spanwise direction but parallel to and away from the jet centerplane will be measured. For this we will use a rake of 16 X-wires in conjunction with 2 rakes of 8 X-wires each, displaced by small distances from the larger rake ($+\Delta y$ and $-\Delta y$ respectively). Variations of ω_y in the z-direction should indicate spanwise wavelike distortions of the nominally spanwise structure (roll) on one side of the jet. These data will be used to determine probe spacing and locations of rakes to study further details of the CS. (2) Having found the most probable wavelength λ of contortion on the spanwise rolls, two-dimensional cuts of spanwise structures will be educed by measuring $\omega_z(y,t)$ simultaneously at three planes $\lambda/2$ apart. The objective of this is to educe details of the rolls, such as their center location, contortion, and inclination in the streamwise direction. (3) Finally, a configuration similar to the first (but with the rakes closer together) will be used to measure the transverse vorticity component $\omega_y(z,t)$ of the longitudinal structures (ribs). The component of ω_y of the inclined rolls will be distinguished from the ω_y component of the ribs based on their relative location along the time coordinate (see Hussain & Hayakawa 1989).

6. Use of 9-Wire Probe in Coherent Structure Detection/Eduction

In our continuing effort to develop techniques for detection and eduction of CS in turbulent flows, we have been working on the implementation of a 9-wire vorticity probe for direct measurement of vorticity signals. In the past year, we have had to fix certain problems associated with the calibration procedure of the probe. We have now split up the calibration routines so as to acquire the requisite data in the first phase and then carry out post-processing of that data to obtain calibration coefficients. We have also designed a new traverse system to achieve 'actual' pitch

calibration of the probe. (In the previous setup, the pitch calibration was carried out by rotating the probe 90 degrees about its axis and then repeating the yaw calibration.) At present, we are at the validation stage with respect to the modified calibration routines; following this, we will conduct a study of the statistics of vorticity and helicity in the near field of an axisymmetric jet.

With the intention of fabricating new multi-wire probes in-house, we have identified our requirements and are at a stage of dealing with vendors to purchase components for assembling a manipulator unit to keep (twelve or more) support prongs at distances of the order of fractions of a millimeter apart.

7. Self-Similar Instability of a Mixing Layer

We have proposed and examined a new approach for the spatially developing mixing layer which takes into account the self-similar nature (due to absence of a characteristic length scale) of the flow. Self-similar spectral modes are used for the Fourier decomposition of disturbances. Their wavenumber and frequency decrease downstream in inverse proportion to the distance. As the first step, the linear development of such modes was studied in a vortex sheet behind a wedge. The self-similar form of disturbances, together with an impermeable wall boundary condition, allowed us to obtain effects of stabilization and phase speed increase of long-wave disturbances which are observed experimentally. Using a far-field approximation, the dispersive equation was derived analytically. In the short-wave limit, our results coincide with Kelvin's. Two particular flows — behind a splitter plate and backward facing step — were studied in detail.

8. Mode Interactions in Low Aspect Ratio Taylor-Couette Flow

Our studies of the bifurcation behavior of low aspect ratio Taylor-Couette flow (in the context of a three dimensional parameter space, where the parameters are Reynolds numbers based on the angular velocities of the inner and outer cylinders [R_i and R_o respectively] and the aspect ratio Γ, were concluded, and a paper has been submitted to *Physics Review Letters* (Li & Hussain). There exist mode interactions around multi-critical points on the locus of the first transition from simple azimuthal flow to Taylor Vortex Flow (TVF) modes. We studied experimentally the more complex states which emerge near these multi-critical points. Future work in this area will include laser Doppler anemometer (LDA) measurements to obtain greater detail of the flow dynamics of the various modes observed in the just-concluded work.

9. Numerical Simulations of Temporally-Evolving Jets and Isolated Vortices

We investigated several fundamental flows of practical interest using direct numerical simulations. These temporal simulations of circular and elliptic jets were motivated by a desire to gain fundamental insight into the formation, evolution, and dynamics of coherent structures in jet flows as well as the need for detailed information about the mechanisms involved in aerodynamic noise, turbulence production, mixing, and entrainment in these flows. In addition, circular and elliptic rings were simulated in isolation to provide complementary information and to get a clear picture of coherent structure dynamics early in the flow evolution. The incompressible Navier-Stokes equations were solved by a spectral (Galerkin) method with a fourth-order predictor-corrector scheme for time-stepping.

We have analyzed our temporal jet simulations by computing the complex helical wave decomposition of the vorticity field. This decomposes the vorticity field into infinitely many left-handed and right-handed Beltrami flows; these basis functions are solutions of the Navier-Stokes equation and form a complete set of orthogonal functions. The superposition of all left- (or right-) handed basis functions constitutes the left- (right-) handed vorticity components of the flow (*i.e.*, the generalized Helmholtz decomposition). For the circular jet, the left- and right-handed components match pointwise in magnitude initially, so there are no helical structures; this remains so through the roll-up and pairing of vortex rings in the shear-layer domain. However, when the jet column mode is reached, the rings develop azimuthal instabilities which eventually result in their total breakdown, and their left- and right-handed vorticity components separate in space. After breakdown, the domain is subsequently filled with mainly streamwise lobes, each one dominated by left- (or right-) handed vorticity, and the total helicity in the domain begins clearly to deviate from zero, indicating differences in the evolution of left- and right-handed components. We assert that this generation of total helicity must be a viscous process, since the rate of change of total helicity must always be zero in the inviscid case. In fact, it is a result of changes in the vortex line topology.

Generalizing, we show that the generation of non-trivial topology as well as non-zero total helicity is typical in viscous flows that are free from constraining geometrical symmetries. Furthermore, it appears that filament-like knotting or linking of entire vortices have vanishing impact on the Beltramization of the flow

in the limit of infinitesimal vortex core size. While vortex collisions and vortex reconnections are important mechanisms for helicity generation, simple viscous decay of well-separated vortical structures can also produce helicity. Furthermore, helicity generation has been found to be very sensitive to Reynolds number; therefore, the application of eddy viscosities and artificial viscosities in large-eddy simulations has questionable faithfulness to the local flow topology. It is not certain the extent to which this may affect the ability of these methods to predict the global dynamics of large-scale structures.

In conclusion, we have studied the dynamics of jet breakdown into turbulence in terms of helical vorticity components; one result is that as vortex ring breakdown occurs in jets, the helical components of vorticity separate spatially. Other simulations have generalized our knowledge of the production of helicity in coherent structure dynamics. We have found that clean linking of vortices is probably not a dominant mechanism in helicity generation because in the thin core limit, knottedness has no impact on the degree of Beltramization of the flow, and yet vortices do not link cleanly unless they have very thin cores. Coherent structures in general do not appear to have trivial topology or zero helicity; when waves form on the vortex rings in a jet, for example, the polarized vorticity components tend to separate spatially.

10. Symmetry breaking in vortex-source and Jeffery-Hamel flows

The stability and bifurcations associated with the loss of azimuthal symmetry of planar flows of a viscous incompressible fluid, such as vortex-source and Jeffry-Hamel flows, are studied by employing linear, weakly nonlinear and fully nonlinear analyses, and features of new solutions are explained (Goldshtik, Hussain & Shtern 1991). We have addressed steady self-similar solutions of the Navier-Stokes equations and their stability to spatially developing disturbances. By considering bifurcations of a potential vortex-source flow, we find secondary solutions. They include asymmetric vortices which are generalizations of the classical point vortex to vortical flows with non-axisymmetric vorticity distributions. Another class of solutions we found relates to transition trajectories that connect new bifurcation-produced solutions with the primary ones. Such solutions provide far-field asymptotes for a number of jet-like flows.

11. Collision of two vortex ring

This work is motivated by our speculation that reconnection of vortices is a frequent event in turbulent flows and that it plays important roles in mixing, and generation of helicity, enstrophy and aerodynamic noise. The interaction of two identical circular viscous vortex rings starting in a side-by-side configuration is investigated by solving the Navier -Stokes equation using a spectral method with 64^3 grid points (Kida, Takaoka & Hussain 1991). This study covered initial Reynolds numbers (ratio of circulation to viscosity) up to 1153. The vortices undergo two successive reconnections, fusion and fission, as has been visualized experimentally, but the simulation shows topological details not observed in experiments. The shapes of the evolving vortex rings are different for different initial conditions, but a mechanism of the reconnection is explained by *bridging*(Melander & Hussain 1988) except that the bridges are created on the front of the dipole close to the position of the maximum strain rate. Spatial structures of various field quantities are compared. It is found that domains of high energy dissipation and high enstrophy production overlap, and that they are highly localized in space compared with the regions of concentrated vorticity. It is shown that the time evolution of concentration of a passive scalar is quite different from that of the vorticity field, confirming our longstanding warning against relying too heavily on flow visualization in laboratory experiments for studying vortex dynamics and coherent structures.

12. Study of velocity, vorticity and helicity of inviscid fluid elements

Recent research in turbulence has been greatly helped by studying the dynamics and motion of particular vortical regions of the flow. To make the best use of vortex dynamics for improving our understanding and interpreting the computation of vortex interactions, it is important to use as effectively as possible the basic results connecting the vorticity ω and the velocity $\mathbf{u}$ of fluid elements as they move, and the conservation conditions involving the integral of helicity density $\mathbf{u}.\omega$. In this study, we have given description, with a new geometrical derivation, of the changes in velocity, vorticity and helicity of fluid elements and fluid volumes in inviscid flow. When a compact material volume V_b moves with a velocity v_b in a flow which at infinity has a velocity U and uniform vorticity Ω, it is shown that in general there is a net change ΔH_E in the integral of helicity H_E in the external region V_E outside the volume, i.e. $H_E = \int_{V_e} \mathbf{u}.\omega dV$ changes by ΔH_E , where $\mathbf{u}$ and ω are the velocity and vorticity fields. When the vorticity at infinity is weak and when Ω is

parallel to v_b and U , the change in the external helicity integral, ΔH_E is proportional to the dipole strength of V_b. Using these results along with symmetry condition, we have developed some new physical concepts about helicity in turbulent flows, in particular concerning the helicity associated with eddy motions in rotating flows and the relative speed E_b of the boundary defining a region of turbulent flow moving into an adjacent region of weak or non-existing turbulence (Hunt & Hussain 1991).

13. Kinematic Separation of Mixtures

Our experience in vortex flows and the mechanics of dispersed mixtures along with their visualization have led us to conjecture that kinematic separation of an initially uniform mixture is possible. We have studied such separation process in a vortex breakdown chamber, consisting of a glass cylinder and two bounding top and bottom plates. The top plate, whose height is adjustable, is fixed to the cylinder for this experiment. The bottom plate and the cylinder can be rotated independently in either direction. When a well-mixed homogeneous mixture of smoke and air is set into motion by rotating the bottom plate, initially a nonuniform distribution of flow markers develops, and when the steady state is reached, the vortex breakdown region becomes depleted of smoke. Since the observed separation of species occurs at a much lower rotational speed than it is required to have separation due to centrifugal action, we came to the conclusion that such separation occurs due to kinematic action (Goldshtik, Husain & Hussain 1992).

REFERENCES

ANTONIA, R.A., CHAMBERS, A.J., BRITZ, D. & BROWNE, L.W.B. 1986 *J. Fluid Mech.* **172**, 221.

BRIDGES, J. & HUSSAIN, F. 1989 in *"Whither Turbulence"* (*Lecture Notes in Physics* **136**) Springer.

BRIDGES, J. 1990 Ph. D. dissertation, University of Houston.

BROZE, J.G., JENKINSON, J.P., & HUSSAIN, F. 1987 *Bull. Am. Phys. Soc.* **32**, 2064.

BROZE, J. G., HUSSAIN, F. & BUELL, J. C. 1988 *CTR-88 Summer Report*, 1.

BROZE, J. G. 1992 Ph.D. dissertation, University of Houston (in progress).

CHOMAZ, J.M., HUERRE, P., & REDEKOPP, L.G. 1988 *Phys. Rev. Lett.* **60**, 25.

GOLDSHTIK, M., HUSAIN, H. & HUSSAIN, 1992 *Physical Review A* (to appear).

GOLDSHTIK, M., HUSSAIN, F. & SHTERN, V. 1991 *J. Fluid Mech.* **232**, 521.

GRASSBERGER, P. & PROCACCIA, I 1983 *Physica* **9D**, 189.

GRINSTEIN, F.F., ORAN, E.S., & BORIS, J.P. 1990 *Phys. Rev. Lett.* **64**, 8.

HUNT, J. C. R. & HUSSAIN, F. 1991*J. Fluid Mech.* **229**, 569.

JENKINSON, J.P. & HUSSAIN, A.K.M.F. 1987 *Bull. Am. Phys. Soc.* **32**, 2026.
JENKINSON, J.P. & HUSSAIN, F. 1990 *Bull. Am. Phys. Soc.* **35**, 2242.
JENKINSON, J.P., HUSAIN, H.S., & HUSSAIN, A.K.M.F. 1984 *Bull. Am. Phys. Soc.* **29**, 1562.
HAYAKAWA, M. & HUSSAIN, F. 1987 *J. Fluid Mech.* **180**, 193.
HAYAKAWA, M. & HUSSAIN, F. 1989 *J. Fluid Mech.* **206**, 375.
HUSSAIN, A. K. M. F. 1983 *Phys. Fluids* **26**, 2816.
HUSSAIN, A. K. M. F. 1986 *J. Fluid Mech.* **173**, 303-356.
KIDA, S., TAKAOKA, M. & HUSSAIN, F. 1991 *J. Fluid Mech.* **230**, 583-646.
KOSTELICH, E. J. & YORKE, J. A. 1988 *Phys. Rev. A* **38**, 1649.
LINDGREN, E.R. 1957 *Arkiv Fysik, Stockholm* **12**, 1.
LUMLEY, J. L. 1967 *Atmospheric Turbulence and Radio Wave Propagation* (eds. Yaglom & Tatarsky), Moscow, NAUKA.
MELANDER, M. & HUSSAIN, F. 1988 'Cut and connect of two antiparallel vortex tubes.' *Center for Turbulence REscarch Proc. Summar Program* 1988.
MONKEWITZ, P. & HUERRE. P. 1990 *Ann. Rev. Fluid Mech.* **22**, 472.
MUMFORD, J.C. 1982 *J. Fluid Mech.* **118**, 241.
PACKARD, N.J., CRUTCHFIELD, J.P., FARMER, J.D., & SHAW, R.S. 1980 *Phys. Rev. Let.* **45**, 712.
RUELLE, D. & TAKENS, F. 1971 *Commun. Math. Phys.* **20**, 167.
SARPKAYA, T. 1966 *Trans. ASME: J. Basic Engng.* **88**, 589.
SCHUSTER, H. G. 1989 *Deterministic Chaos*, VCH Publishers, New York.
STETTLER, J.-C., & HUSSAIN, F. 1986 *J. Fluid Mech.* **170**, 169.
TAKENS, F. 1980 *Proc. Warwick Symp. on Dynamical Systems and Turbulence*, (Springer-Verlag *Lecture Notes in Math.*, **898**), 367.
TSO, J. & HUSSAIN, F. 1989 *J. Fluid Mech.* **203**, 425.
WYGNANSKI, I.J., & CHAMPAGNE, F. 1973 *J. Fluid Mech.* **59**, 281.